UDC 551.513.1:551.521:551.588.1:551.509.313

Response of the Joint Ocean-Atmosphere Model to the Seasonal Variation of the Solar Radiation

RICHARD T. WETHERALD and SYUKURO MANABE
Geophysical Fluid Dynamics Laboratory,[1] NOAA, Princeton, N.J.

ABSTRACT—The effect of the seasonal variation of solar radiation is incorporated into the joint ocean-atmosphere model developed at the Geophysical Fluid Dynamics Laboratory of the National Oceanic and Atmospheric Administration, and the resulting system is integrated for the 1½-yr model time. The purpose of this study is to analyze the response of the joint air-sea model to seasonal changes in the solar zenith angle rather than to obtain a true equilibrium state. Comparisons are also made with results previously presented for the case of annual mean conditions.

The most important feature that emerges as a direct result of this seasonal variation is a significant warming of the lower troposphere in high latitudes. This warming is found to be caused by (1) the removal of the snowpack during the summer season, which decreases the earth's albedo there during this time, and (2) a net rise in the temperature of the ocean surface in high latitudes as a result of the seasonal variation of convective activity in the surface layer of the ocean. The present results indicate that the snow cover effect is the primary factor responsible for this warming trend whereas the ocean effect is of secondary importance.

The main consequences of this high latitude warming include a reduction of the mean atmospheric north–south temperature gradient (and, therefore, a reduction of baroclinic instability in middle latitudes), a reduction of the mean oceanic meridional circulation, and a reduction of the atmospheric and oceanic poleward heat energy transports.

1. INTRODUCTION

In recent years, a mathematical model of the joint ocean-atmosphere system was constructed by Bryan and Manabe at the Geophysical Fluid Dynamics Laboratory of the National Oceanic and Atmospheric Administration (NOAA). An attempt was made to investigate the problem of ocean-atmosphere interaction by performing a series of controlled numerical experiments. This was done in the following stages:

1. A study of an atmospheric model without the effect of ocean circulation,
2. A study of the ocean model without any feedback effect from the atmosphere, and
3. A study of the joint ocean-atmosphere model in which the two systems are allowed to interact fully with each other.

In all three stages, an annual mean distribution of solar radiation was used. The details of these studies are given in Manabe (1969*a*, 1969*b*) and in Bryan (1969).

This present study is a continuation of the joint ocean-atmosphere project and constitutes a preliminary investigation of the response of the ocean-atmosphere system to the seasonal variation of solar radiation. The purpose of the study is to determine how the annual mean state obtained by Bryan and Manabe is modified by this seasonal variation. The differences between this time mean state and the one obtained with a seasonal variation should yield some insight as to how the climate of the earth is affected by seasonal fluctuations of solar radiation.

Due to limitations of computer time, we decided to analyze only the response of the ocean-atmosphere system to this seasonal variation rather than to run longer and obtain a true equilibrium state. In the course of this analysis, many interesting features emerged, but the most important of these was the significant warming trend obtained when seasonal variations were considered. No comparable warming trend appeared in the annual mean state. We, therefore, decided to concentrate mainly on this aspect of the results and to postpone the description of other features until a more detailed and refined seasonal study is made.

It should be made clear that equilibrium is not obtained in any part of the region of the integration but that the troposphere and the shallow portion of the ocean are probably the nearest to this state. Here, we shall refer to the model studied by Manabe (1969*b*) and Bryan (1969), as the "annual mean model" and the current experiment as the "seasonal model."

2. STRUCTURE OF THE MODEL

The joint ocean-atmosphere model consists of two main parts, the oceanic part and the atmospheric part. A very brief description of each part of the model follows.

The atmospheric part of the joint model is the same as that described by Manabe (1969*a*, 1969*b*). Velocity, temperature, water vapor, and surface pressure are calculated at each of the grid points, spaced approximately 500 km apart. Calculations are carried out at nine levels chosen so that they resolve the structure of the lower

[1] At Forrestal Campus of Princeton University

TABLE 1.—*Depth (m) of ocean model levels for both five- and nine-level versions.*

Five levels	Nine levels
67	25
100	50
300	75
1000	100
3000	150
	300
	500
	1000
	3000

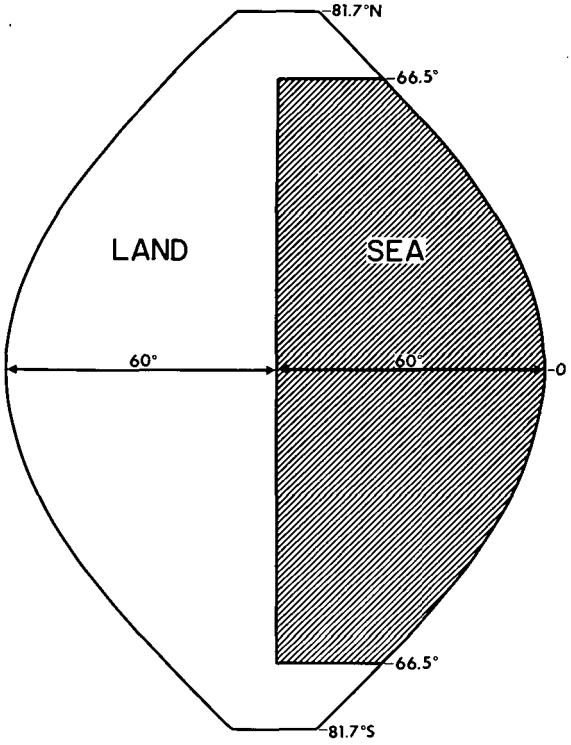

FIGURE 1.—Distribution of the continents and the ocean in the ocean-atmosphere model. Cyclic continuity is assumed at the eastern and western ends of the domain.

stratosphere and the planetary boundary layer. The radiation model is essentially that described by Manabe and Strickler (1964), except that seasonal variations of solar radiation are now taken into consideration. The depletion of solar radiation and the transfer of terrestrial radiation is computed by taking into consideration cloud and gaseous absorbers such as carbon dioxide, water vapor, and oxone. The distributions of cloudiness and carbon dioxide are specified in advance and are held constant. The distributions of water vapor and ozone are specified to correspond to zonal averages taken from climatological data and are made to vary with season. A brief description of the computation of the seasonal variation of the insolation and the variation of the latter two absorbers is given in appendix 1. The distribution of water vapor used in the radiative computation is different from the distribution obtained from the hydrologic part of the model described below. In other words, the radiative computation is "uncoupled" from the computed hydrologic cycle. The consequence of this uncoupling is discussed in section 8. The prognostic equation of water vapor involves the three-dimensional advection of water vapor, condensation, and evaporation. Over continental surfaces, the depth of snow cover and the amount of soil moisture are based upon detailed balance computations of snow and soil moisture, respectively. In particular, the snow depth is increased by snowfall and depleted by evaporation and snowmelt. The latter quantity is computed from the requirement of the heat balance when conditions for the snowmelt are satisfied. Differentiation between rain or snow is determined by the temperature at a height of approximately 350 m. If this temperature is at freezing or below, snow is predicted; otherwise, rain is forecast. Surface albedos are the same as those described in Manabe (1969*a*). An albedo of 70 percent is assigned to those continental areas which are covered by snow.

The oceanic part of the joint model is basically the same as that described in Bryan (1969). Fields of velocity, temperature, and salinity are calculated explicitly, and density is calculated from an equation of state. Calculations are, however, carried out for nine rather than for five levels with respect to the vertical coordinate to obtain better vertical resolution in the ocean model, particularly in the upper layers. For the sake of comparison, the vertical structure for both versions is shown in table 1.

The calculations are carried out for a region on a globe bounded by two meridians 120° of longitude apart. Cyclic continuity is assumed for the atmosphere at these meridional boundaries. The regions immediately adjacent to the poles are excluded by free slip, insulated walls at 81.7°N and 81.7°S. In the interval between 66.5°N and 66.5°S, half of the area is covered by ocean. Figure 1 shows this ocean-continent distribution. For the full details of both the atmosphere and ocean models, the reader is referred to Manabe (1969*a*, 1969*b*) and Bryan (1969), respectively. Hereafter, these studies will be referred to simply as parts I, II, and III. [For a simplified version of these studies, see Manabe and Bryan (1969).]

3. INITIAL CONDITIONS AND TIME INTEGRATION

For the case of annual mean insolation, the coupling between the atmospheric part and the oceanic part of the model was adjusted so that the evolution of the former during 1 atmospheric yr interacted with that of the latter during 100 oceanic yr. In other words, 1 yr of integration of the atmospheric model was performed concurrently with 100 yr of integration of the oceanic model. This was done to optimize the amount of computation required for reaching a quasi-equilibrium state.

The initial starting point for the present study was taken to be near the end of the 1-yr, joint annual mean

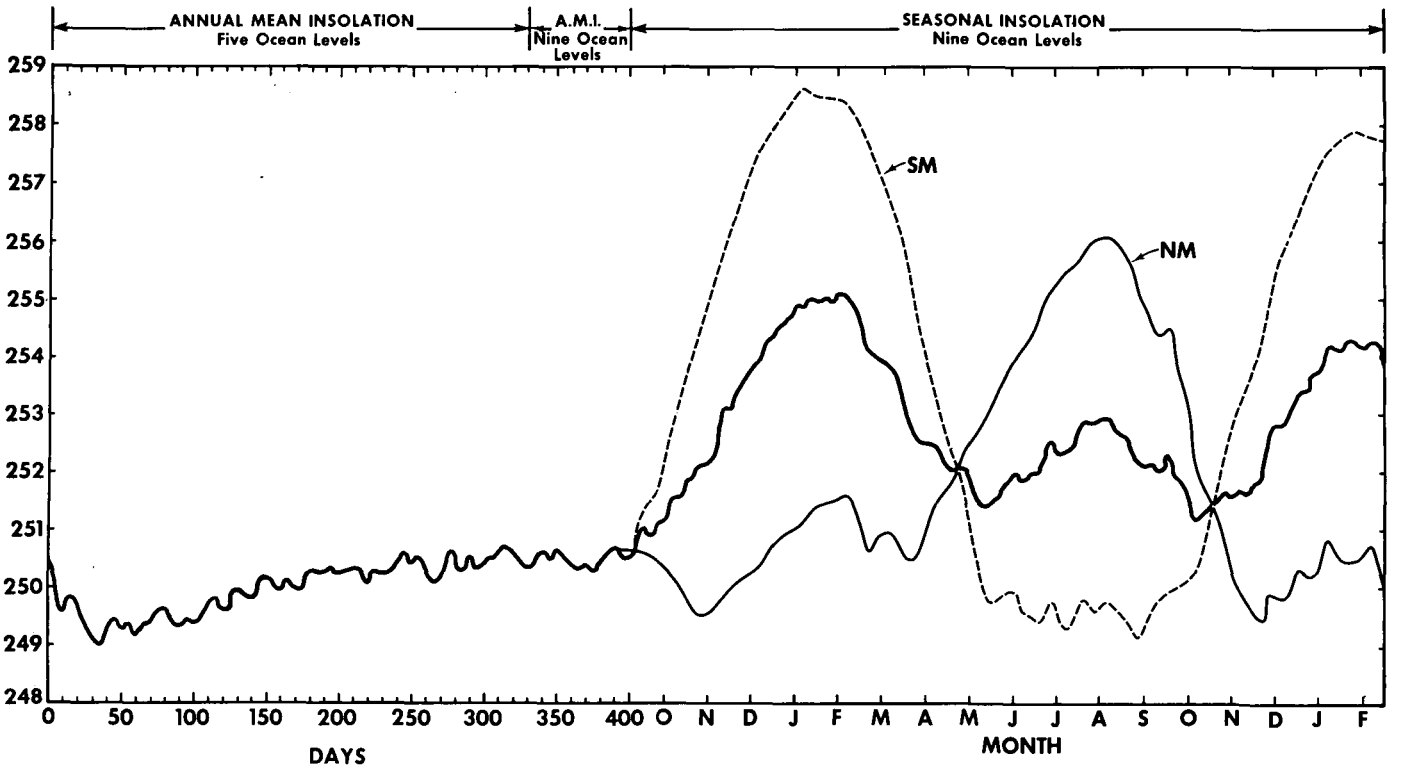

FIGURE 2.—Time variation of atmospheric potential energy (10^3 J·cm^{-2}) for the entire period of the time integration of the joint ocean-atmosphere model. The total potential energy is represented by a solid heavy line, the Northern Hemisphere mean potential energy (NM) by a thin solid line, and the Southern Hemisphere mean potential energy (SM) by a thin dashed line.

model period (100 yr of ocean time). At this point, the number of ocean levels was increased from five to nine. After this change, the model was run in an annual mean state for 65 model atmospheric days (or approximately 18 oceanic years) to adjust the ocean model to the new vertical computational resolution. At the end of this period, the annual mean insolation was changed to a seasonal variation and the run continued in this manner for approximately 1½ yr of model time. The astronomical starting point for the seasonal stage was taken to be 0000 GMT on Sept. 23, 1962. Also, the ratio of the time synchronization between the atmosphere and ocean models was reset to unity; that is, 1 day of atmospheric time corresponds to 1 day of ocean time.

At the beginning of the seasonal model run, the snow depth was reset to 1 cm water equivalent whenever it was greater than this value. This was done to avoid starting the seasonal computation with the arbitrary snow depth that was present at the end of the annual mean model run.

The computer program for the seasonal model contained the same wind stress error discussed in part II.[2] Since this inconsistency was examined and found to have a minor effect upon the thermal structure of the model, we felt that this error would not alter significantly the essential features of the results obtained from the seasonal computation.

[2] Toward the end of the integration of the seasonal model, it was discovered that the stress values used as an upper boundary condition for the ocean were multiplied by an extraneous factor, the cosine of the latitude. This error was present in both the seasonal and annual mean models.

Figure 2 illustrates the total sequence of events; that is, the entire time series of the mass integral of atmospheric potential energy from the beginning of the time integration of the annual mean model to the end of the integration of the seasonal model. For the case of flat terrain, the expression for the total potential energy, averaged over the computational domain A, is given by

$$\mathrm{PE}=\frac{1}{A}\int\left(\frac{1}{g}\int_0^{p_*} c_p T dp\right) dA$$

where PE is potential energy, g is gravity, c_p is specific heat of air under constant pressure, T is temperature, p_* is surface pressure, and p is pressure. (Note that total potential energy is proportional to the mean atmospheric temperature.) Figure 2 clearly shows the previously mentioned strong warming trend in the seasonal model atmosphere that does not occur in the annual mean model atmosphere. In the seasonal portion of this figure, the potential energy curves for the two model hemispheres are shown separately, in addition to the total potential energy integral. The differences in amplitude between the two model hemispheres are due to the transient effect caused by the starting procedure; that is, the Northern Hemisphere experiences the winter season first whereas the Southern Hemisphere experiences the summer season first. Since the amplitudes of the seasonal portion of the potential energy curves are changing with time, it is obvious that the seasonal model atmosphere is still in a transient state rather than in an equilibrium state.

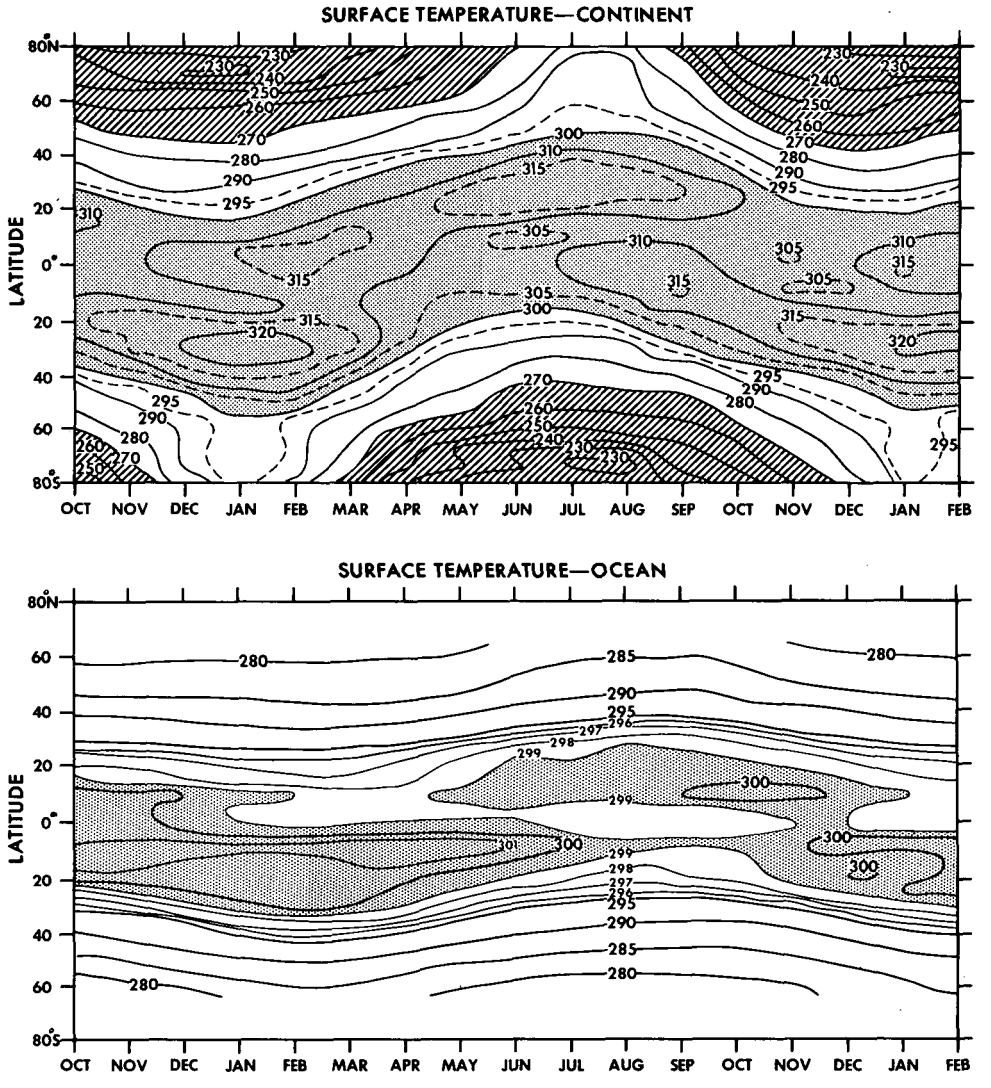

FIGURE 3.—Time variation of zonal mean surface temperature (°K) for both continent and ocean, separately. The entire period of the seasonal integration is shown.

Figure 2 also shows the transition period between the five- and nine-level ocean models. Note that the integral of potential energy was affected very little by this change in the number of ocean levels.

4. SEASONAL VARIATION

To illustrate the nature of the seasonal time integration, the time variations of four fundamental quantities are presented. These quantities are (1) the temperature of the continental and oceanic surfaces, (2) the temperature of the ocean interior, (3) the rate of precipitation over the continent and the ocean, and (4) the stream function of the meridional circulation in the model.

Surface Temperature

Figure 3 shows the time series of monthly means of the zonally averaged surface temperature for land and sea separately (upper and lower portions of figure, respectively). This and subsequent time series cover the entire period of the seasonal integration. The amplitude of the variation of the surface temperature is much greater over the land than over the sea since the land is assumed to have no heat capacity, and hence is more sensitive to changing thermal influences than the ocean. As expected, the maximum temperatures are found in the summer hemisphere. For the continent, the maximum temperature belt is located at about 30° latitude whereas in the ocean the maximum temperatures are centered at about 10° latitude. The location of this area of higher temperature for the continent is due to the formation of a dry or "desert" region during the summer season, centered at 30° latitude. This dry area implies a large reduction of soil moisture available for evaporation and hence a reduction of evaporative cooling there. Also of interest are the above-freezing temperatures that occur at the continental polar boundaries during the respective summer seasons. These warm polar temperatures will be discussed more fully in sections 5 and 6.

An interesting feature of the ocean surface temperature distribution is the presence of a minimum temperature

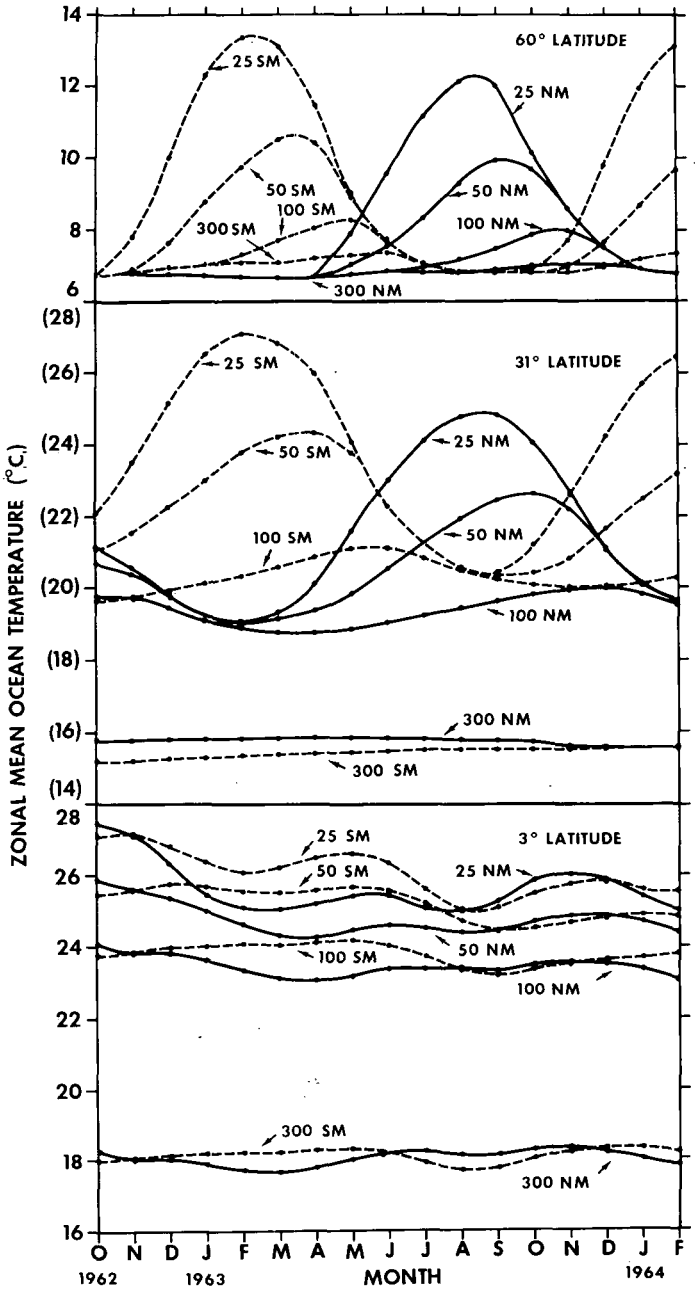

FIGURE 4.—Time variation of zonal mean oceanic temperature (°C) at various depths for both hemispheres at latitudes 60°, 31°, and 3° (from top to bottom), respectively. The entire period of the seasonal integration is shown. The Northern Hemisphere mean values (NM) are represented by solid lines, and the Southern Hemisphere mean values (SM) by dashed lines.

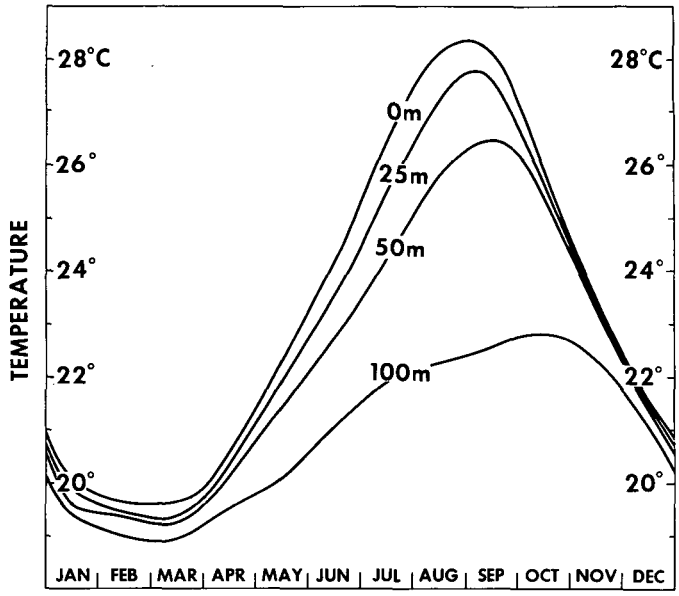

FIGURE 5.—Annual variation of temperature at different depths in the Kuroshio current off the South Coast of Japan. The figure is taken from Sverdrup et al. [(1942), fig. 32B, p. 131].

belt located at the Equator. This temperature minimum is due to the upwelling of cold water at the Equator throughout the entire yearly cycle. This upwelling has already been discussed in parts II and III.

Ocean Depth Temperature

Figure 4 shows the variation of zonal mean oceanic temperature as a function of depth at latitudes 60°, 31°, and 3°, respectively, for both hemispheres. The oceanic model levels displayed are located at 25, 50, 100, and 300 m, respectively. These curves illustrate how the various layers in the oceanic model respond to the seasonal variation of insolation at different latitude regions. They are described below.

Variations at 60° latitude. The relative rates of heating and cooling from one oceanic layer to another are quite different. In general, heating from the surface penetrates downward at a much slower rate than does cooling throughout the same region because the former process is accomplished mainly by turbulent mixing whereas the latter process is governed mainly by free convection. To simulate the effects of free convection, a so-called "convective adjustment" is used (Bryan 1969) in the oceanic model. Whenever the vertical density gradient becomes unstable, it is assumed that the intensity of free convection is strong enough to create a layer of neutral stability instantaneously. For further details of this adjustment, see part III.

In the figure for 60° latitude, all four levels show a response to the annual variation of solar radiation, but that response is slower and less pronounced with depth. Below 300 m, there is little or no response to surface temperature changes. Cooling by the convective adjustment proceeds at approximately the same rate at all levels in the convective layer.

Variations at 31° latitude. The situation at 31° latitude differs from that at 60° in that the response extends down to only the 100-m oceanic level. Furthermore, the convective adjustment does not quite reach the 100-m oceanic level whereas, in the higher latitude belt, all four levels were affected to some extent by this mechanism. As in the case of the potential energy illustration (fig. 2), there are noticeable differences between the amplitudes of the temperature oscillations for the model Northern and Southern Hemispheres. This feature is most apparent in the figure for 31° latitude.

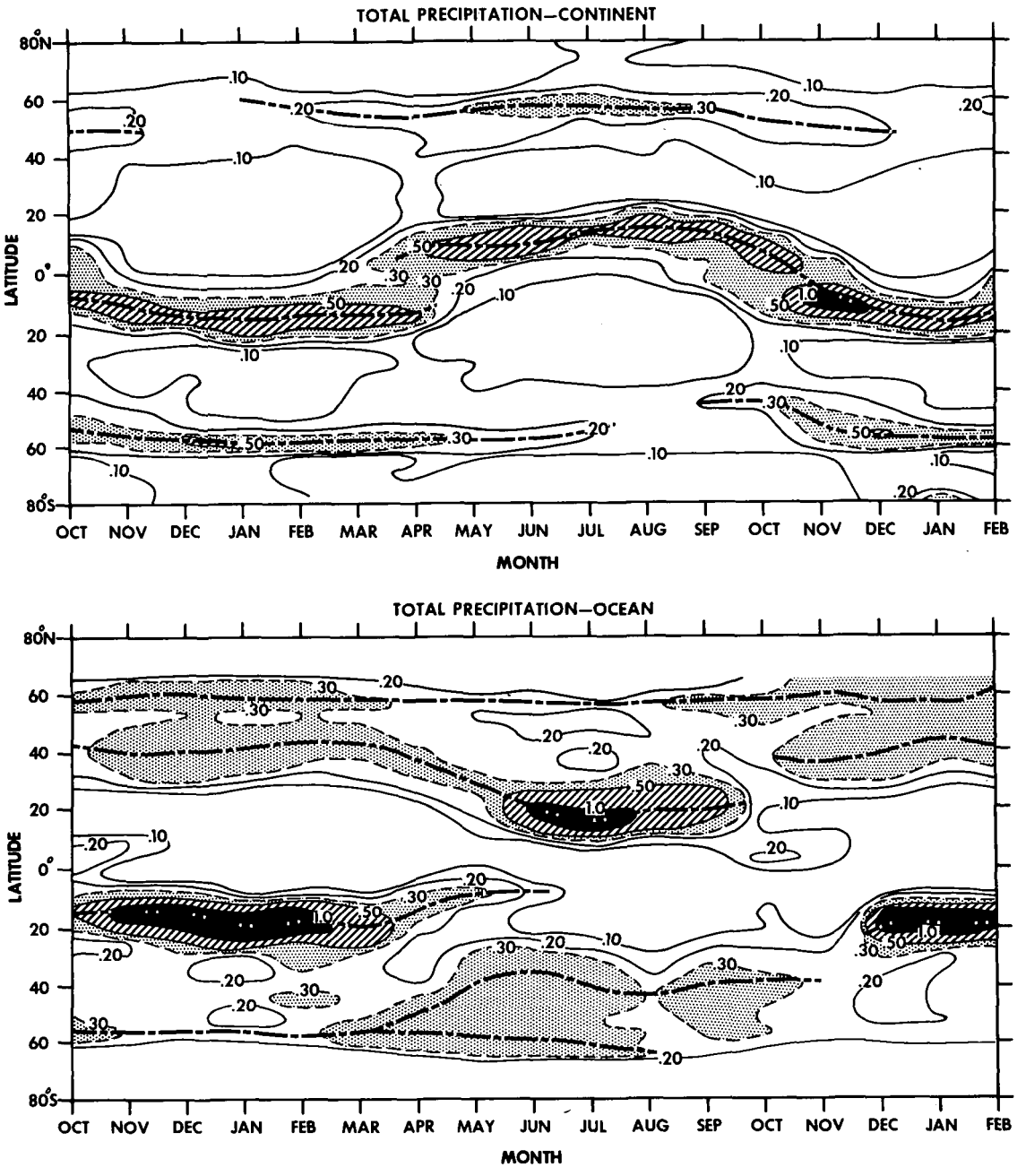

FIGURE 6.—Time variation of total zonal mean precipitation rates (cm/day) for continent and ocean, separately. The entire period of the seasonal integration is shown.

It is interesting to note that the curves shown for the 60° and 31° latitude cases compare favorably in form with selected curves of this type in the literature. Examples of this are given in Sverdrup et al. (1942) and Robinson (1951, 1957). A pertinent illustration from Sverdrup et al. is shown in figure 5. According to the two cited studies by Robinson, this form of average ocean-depth temperature variation appears to be quite prevalent throughout a wide region of the North Pacific Ocean in middle and high latitudes. Exceptions to this comparison are tendencies for double cycles to occur at or below 200 ft (61 m) for the observed temperature variations. These double cycles are not evident in the zonally averaged computed results.

Variations at 3° latitude. The picture at the 3° latitude belt is entirely different from either of the previously described cases. In low latitudes, the oceanic temperatures over the entire 300-m depth have two maxima during a yearly cycle. However, the temperature oscillations are much more in phase with one another than they are in middle and high latitudes. In this region, variations in cold water upwelling driven by the surface wind stress undoubtedly play a more important role than turbulent mixing in determining the temperature variation at different levels. Vertical mixing by the convective adjustment is, for all practical purposes, nonexistent at very low latitudes because of stable stratification of water

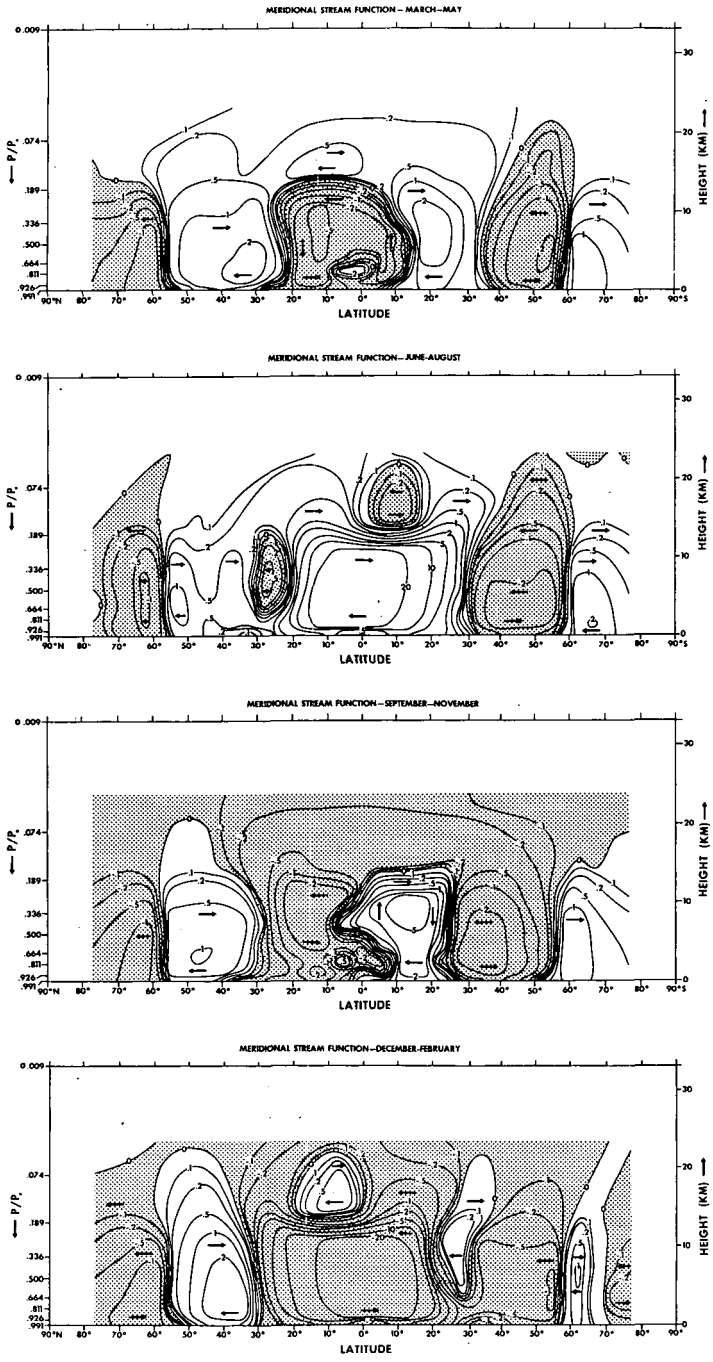

FIGURE 7.—Mean atmospheric stream function of the meridional circulation for the four seasons (average of 3 mo). From top to bottom these are spring, summer, fall, and winter, respectively. Averages are taken over the last full year of the seasonal integration. Units: 1.0×10^{13} gm/s.

masses. A more detailed study of the oceanic circulation in low latitudes as a function of time is necessary, however, to explain this temperature variation more completely.

Precipitation

The distributions of zonal mean rate of precipitation for continental and oceanic regions are given in the upper and lower portions of figure 6, respectively. Both distributions have one feature in common; namely, an intense rainbelt located in the summer hemisphere at tropical or subtropical latitudes. In other respects, however, they are quite different as explained below.

Land distribution. The mean location of the tropical rainbelt over the continent is about 10°–15° latitude during the summer months. Precipitation intensity in the rainbelt is quite uniform throughout most of the year, except during those months when the rainbelt approaches the Equator. The tropical rainbelt becomes less pronounced when it crosses the Equator. This crossing occurs during the months of April and October; that is, in the middle of the transition seasons. Note also that the heaviest precipitation in the middle to high latitudes occurs in the summer hemisphere despite the occurrence of intense cyclonic activity in the corresponding winter hemisphere. This is partly due to the dryness of the continental air mass during the winter season. The summer hemisphere area of precipitation is formed in a relatively narrow band centered at about 55° latitude and is characterized by weak cyclonic disturbances.

Sea distribution. In the mean, the tropical rainbelt over the sea is located slightly poleward of the corresponding rainbelt over the land; namely, at 10°–25° latitude. The rainbelt is wider in a north–south direction but is intense over a much shorter time period. As is apparent from figure 6, the tropical rainbelt over the ocean is completely discontinuous across the Equater where the upwelling of relatively cold water predominates. In middle and high latitudes, the seasonal distribution of precipitation over the sea is the reverse of that over land; that is, the maximum precipitation areas occur in the winter hemisphere and extend over a wide latitude region. This wide area corresponds to relatively intense, large-scale cyclonic disturbances that develop off the east coast of the continent and travel poleward during the colder season.

It should be noted that the belt of cold water upwelling in the equatorial region is too wide, due mainly to the poor resolution of the computational grid network. This wide belt of cold water is probably responsible for the location of the low-latitude oceanic rainbelt in the subtropics rather than in the Tropics of the model.

Meridional Circulation

The meridional atmospheric circulation is the final example in this series of figures showing the seasonal behavior of the model. Figure 7 shows the mean meridional stream function for the four seasons (top to bottom). These seasonal means, constructed by taking the appropriate monthly averages over the last full year of the time integration, are presented to illustrate the seasonal variation of the Hadley circulation. During the months of March, April, and May (Northern Hemisphere spring), the cross-equatorial Hadley circulation is in the process of reversing direction; the Southern Hemispheric cell strengthens as the Northern Hemispheric cell weakens. During the months of June, July, and August (Northern Hemisphere summer), the Southern Hemisphere Hadley cell extends to the Northern Hemisphere, whereas its northern counterpart has practically disappeared. With

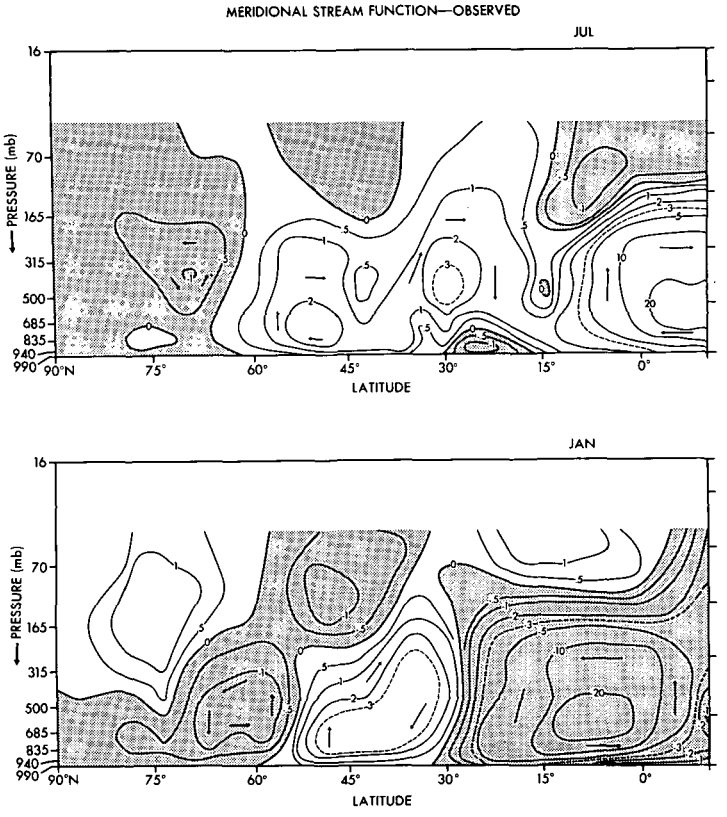

FIGURE 8.—Mean meridional circulation (10^{13} gm/s) for July (top) and January (bottom). Figures are taken from Oort and Rasmusson [(1970), fig. 1, p. 426].

the approach of the Northern Hemisphere winter, the cross-equatorial Hadley circulation again reverses itself, passing through the same stages as before until the Northern Hemisphere Hadley cell now becomes the dominant circulation and its southern counterpart is very small.

In general, the locations of the tropical rainbelts over the land and the sea are directly correlated with the movement and intensity of the upward motion of the ascending branch of the Hadley cell over land and sea. This ascending branch becomes more disorganized during the transition seasons and, therefore, the rainbelt is less intense at these times. This is particularly true over the ocean where downward motion prevails at the Equator as a result of the unrealistically wide pool of cold water there.

Furthermore, during the winter and summer seasons, a small stratospheric indirect cell forms just above the main Hadley cell in the winter hemisphere. It is not certain whether this cell has any correspondence to reality or is simply a result of inadequate resolution of finite differences in the Tropics.

One can compare the present computed results for the extreme seasons with those given by Kidson et al. (1969) and Oort and Rasmusson (1970). The relevant figures from Oort and Rasmusson are reproduced here as figure 8. In both studies, the winter hemispheric Hadley cell is the dominant feature in the tropical meridional circulation. The two Hadley circulations, however, differ in latitudinal extent. In the present computed result, the Hadley cell extends approximately 15°–20° latitude into the summer hemisphere whereas in the study by Oort and Rasmusson, this corresponding extent is only approximately 5°–10° latitude. This is consistent with the remarks made above concerning the location of the tropical rainbelt in the subtropical ocean of the seasonal model.

In the middle latitudes of the summer hemisphere, both computed and observed meridional circulations show a relatively weak and fragmented Ferrel cell while in the winter hemisphere the Ferrel cell is much stronger and better organized.

5. WARMING TREND

In section 3, it is shown that a net warming tendency is obtained for the seasonal model atmosphere as compared to the annual mean model atmosphere. This warming trend is illustrated very clearly by figure 9. The right-hand side of figure 9 shows the latitude-height distribution of tropospheric and upper oceanic difference in zonal mean temperature between the seasonal and the annual mean model states. For reference, the corresponding temperature distribution for the seasonal model is shown in the adjacent left-hand portion of the figure.

Figure 9 shows a general increase of zonal mean temperature over most of the troposphere for the seasonal model. However, this temperature increase is particularly evident in the lower troposphere at high latitudes. There is also a smaller temperature increase in the upper 100 m of the surface layer of the ocean at higher latitudes.

Figure 10 is presented to illustrate the horizontal extent of these temperature increases. The right-hand portion of the figure shows the horizontal distribution of the mean surface temperature difference between the seasonal and annual mean model states. Again, the corresponding temperature distribution for the seasonal model is shown in the left-hand portion of the figure. As expected, the same type of pattern is evident; namely, a large surface temperature increase in high latitudes. It is interesting, however, that the surface temperature increase over the ocean is considerably smaller than that over the continent in the 55°–65° latitude region.

6. CAUSES OF WARMING TREND

Analysis of the seasonal model results suggests that the warming trend, illustrated in the preceding section, was due to two specific factors:

1. The removal of snow cover in high latitudes during the summer season which, in turn, reduces the earth's effective albedo; and
2. A net warming of the ocean surface in high latitudes caused by the seasonal variation of convective activity in the surface layers of the ocean.

This section is devoted to presenting evidence for these two mechanisms.

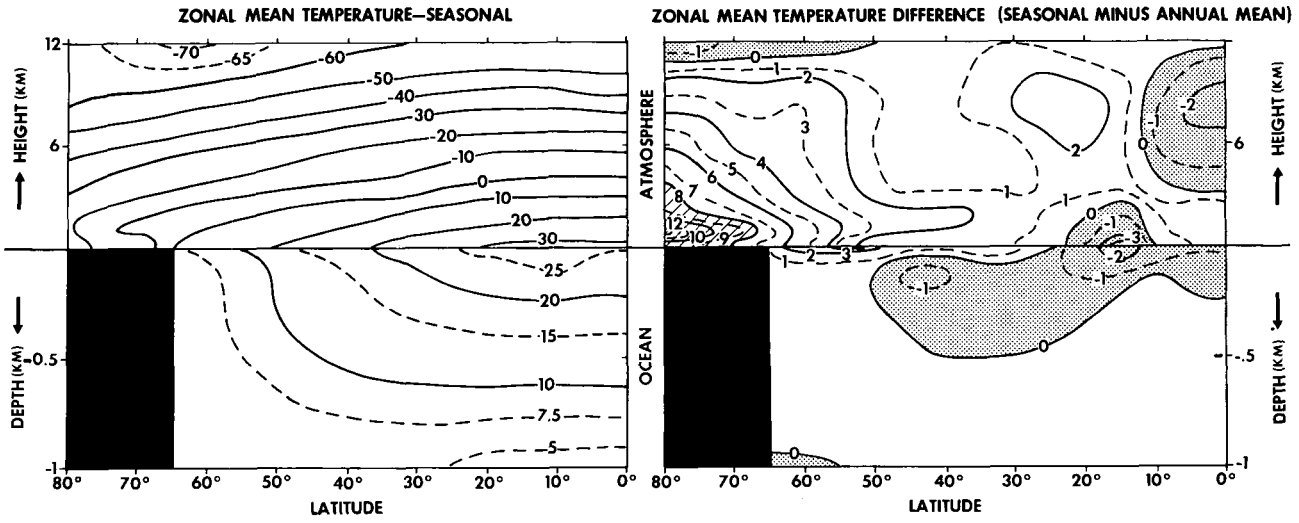

FIGURE 9.—(Right) latitude-height distribution of the zonal mean temperature difference (°C) between the seasonal and the annual mean model states for the tropospheric and upper oceanic parts of the model; (left) the corresponding zonal mean temperature distribution of the seasonal model. Averages are taken over the last full year of the seasonal integration and of the values for the two hemispheres.

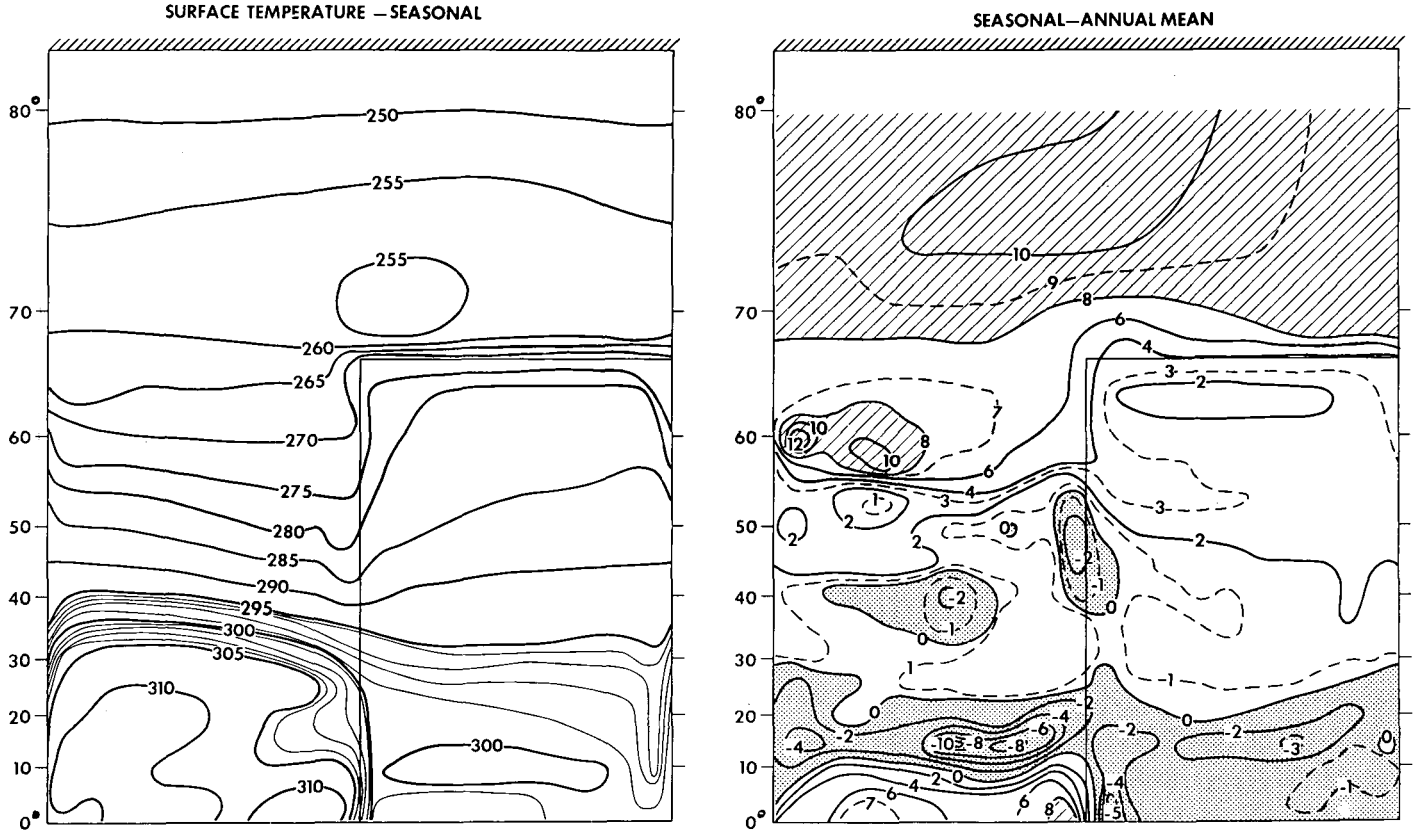

FIGURE 10.—(Left) horizontal distribution of mean surface temperature (°K) for the seasonal model; (right) the corresponding horizontal distribution of the mean surface temperature difference (°K) between the seasonal and the annual mean model states. The averaging procedure is the same as that used for figure 9.

Snow Cover

The upper portion of figure 11 shows the time variation of monthly mean snow depth expressed in terms of water equivalent (cm). As one would expect, the maximum snow depth occurs during the latter portion of the winter season, or even during early spring, depending upon latitude. In general, up to about 70° latitude, the snow depth increases with increasing latitude and snow cover persists for a longer period. Above this latitude, the snow depth falls off sharply, presumably due to the decreased snowfall amounts in these colder regions. In the summer season, the snowpack completely disappears which in turn de-

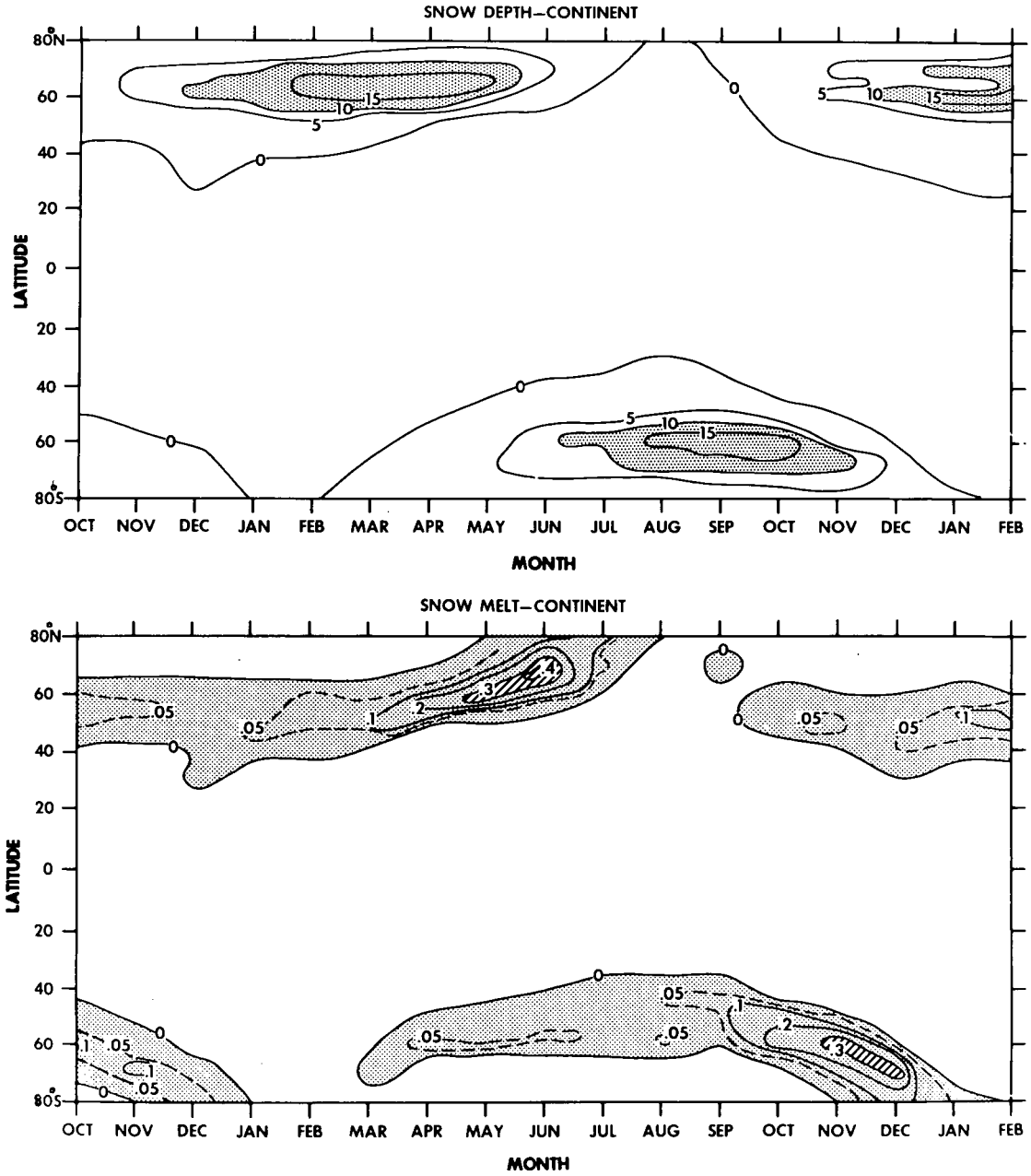

FIGURE 11.—(Top) time variation of monthly mean snow depth in water equivalent (cm); (bottom) time variation of rate of snowmelt in cm of water equivalent per day.

creases the surface albedo from the snow cover value of 70 percent to the value for bare soil.

Another interesting feature contained in the snow depth illustration is the rate of accumulation and disappearance of the snowpack or snow cover. The snowpack builds up slowly but disappears quite rapidly. This is caused by the rapid rate of the snowmelt process in the spring and early summer seasons and the slower snowpack accumulation resulting from snowfall. The details of the snowmelt process are given in part I.

The lower portion of figure 11 shows the distribution of the rate of snowmelt in water equivalent as a function of season. As the figure indicates, snowmelt was present mainly during the spring and early summer months depending upon latitude; the maximum occurring between 60° and 70° latitude. The high rate of snowmelt in this period accounts for the rapid disappearance of the snowpack. In the seasonal computation, the snowmelt process extends all the way to the northern or southern boundaries as opposed to the case of the annual mean model where snow melt was present only along a 20° latitude belt nearest the edge of the snowpack.

Another illustration of the snow hydrology of the seasonal model is presented in figure 12. The upper and lower portions of this figure show the snow budget diagrams for both the annual mean and the seasonal models, respectively. The snowpack for the seasonal model shows very little net accumulation over a year's period, compared to

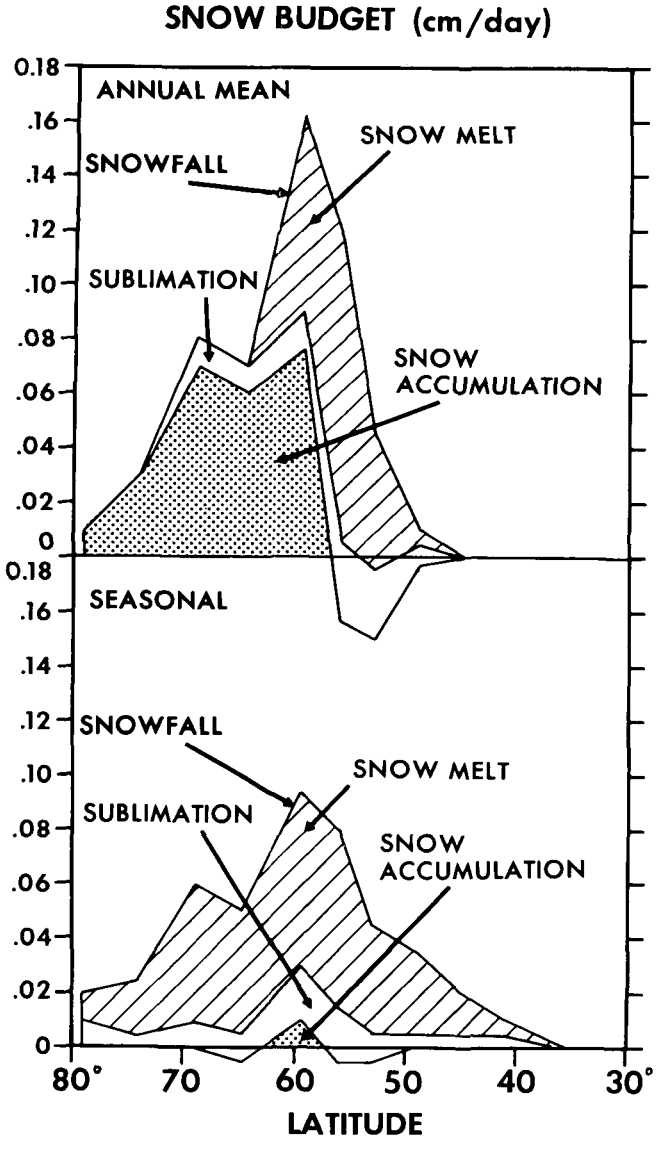

FIGURE 12.—Latitudinal distributions of zonal mean rates of various snow budget components (snowfall, snowmelt, and sublimation) on the continental surface. The rate of snowfall is equal to the sum of the snow budget components shown. Units: cm of water equivalent per day.

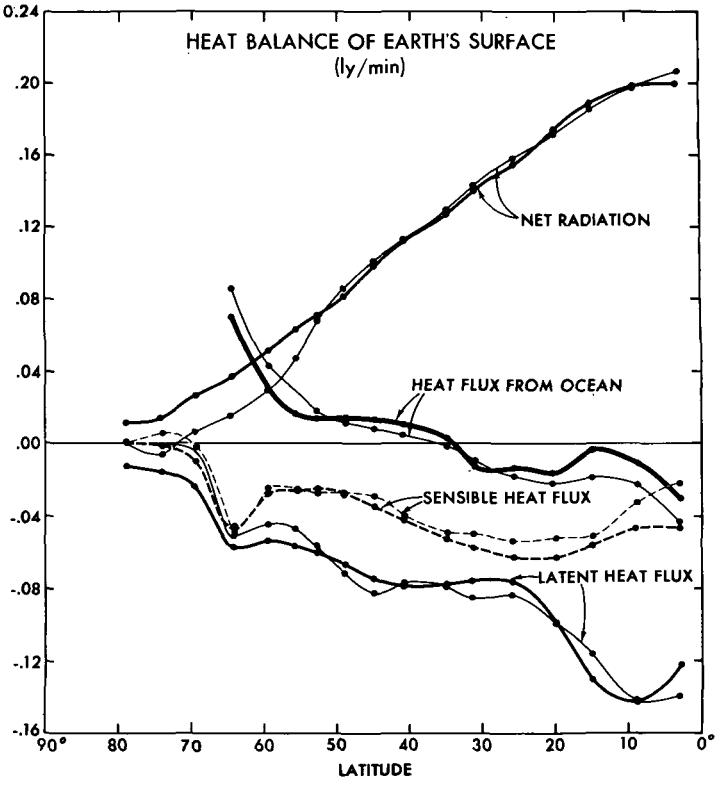

FIGURE 13.—Zonal mean rates of heating (ly/min) of the model surface (both land and sea together), due to net radiation, latent heat flux, sensible heat flux, and heat flow from the interior to the surface of the model ocean. Thick lines indicate the results from the seasonal model ocean. Thin lines indicate the results from the annual mean model.

that of the annual mean model, because the snowpack completely melts during the summer months.[3] Also evident in figure 12 is the apparent lower annual snowfall amount in the seasonal model. This is due to the increased mean temperature in high latitudes caused by the two factors mentioned previously. Because of the temperature increase, snowfall accounts for a smaller fraction of the precipitation in the seasonal model than in the annual mean model.

As was shown earlier, the snowmelt process for the seasonal model extends over the entire width of the snowbelt and represents the dominant mechanism for reducing the snowpack. In general, sublimation (evaporation) was found to be a relatively inefficient method for reducing the snowpack regardless of the season. One should note that the snowline extends further equatorward in the present result because of the cold winter temperatures obtained for the seasonal model.

Section 9B of part II contains a rather complete discussion of the heat balance of the earth's surface. One of the main differences between the results cited there and those obtained by Budyko (fig. 45B of part II) is the relative smallness of all the heat balance components poleward of about 60° latitude over the continent computed for the annual mean study. The cause of this discrepancy was speculated to be the excessive snow cover over the continent. This tended to minimize the surface net downward radiation in high latitudes.[4] Figure 13 shows the comparison between the seasonal and annual mean models, averaged over land and sea, for these components. The main difference between the two results is in high latitudes. Since the seasonal variation of the solar radiation acts to remove the snowpack during the summer months, the net radiation at the surface now has a significant positive value in high latitudes. This net radiation increase is mainly compensated for by the latent heat flux. The present net radiation and latent heat flux curves

[3] Due to an oversight, the mechanism for iceberg formation (removing snowpack in excess of 20 cm water equivalent and considering this excess of snow as "ice runoff") that was incorporated into the annual mean model was retained in the seasonal model integration. Therefore, the small net accumulation around 60° latitude represents this excess snowpack that was given to the ocean model.

[4] Net downward radiation is defined here as the difference between net downward solar radiation and net upward longwave radiation.

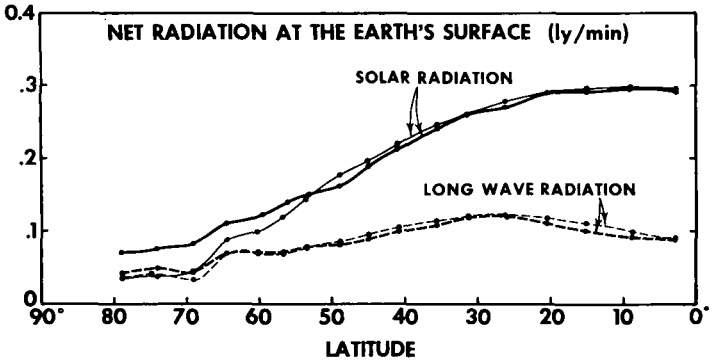

FIGURE 14.—Zonal mean rates of net downward solar radiation and net upward longwave radiation from the seasonal model (thick lines) and from the annual mean model (thin lines). Units: ly/min.

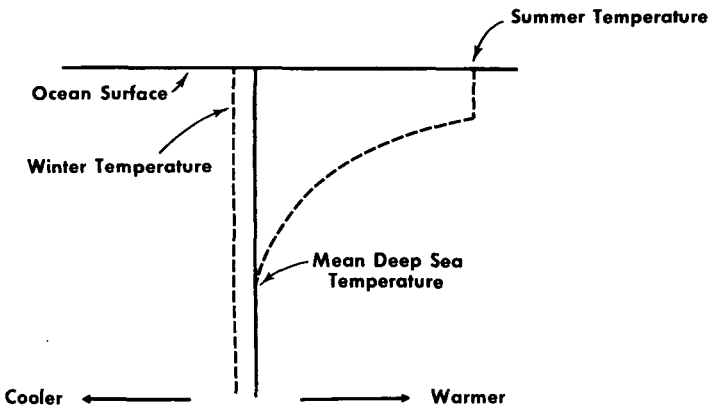

FIGURE 15.—Schematic diagram showing how the ocean is heated or cooled at high latitudes.

are in better qualitative agreement with the trend of Budyko's (1963) results, although his study does not extend to 81° latitude. The heat flow from the interior to the surface of the polar ocean has been reduced slightly but is still high in comparison to Budyko's result (fig. 46 of part II).

For further clarification, the net radiation curve in figure 13 is broken down into its two separate components in figure 14. The solar radiation curves clearly show a net increase of this quantity in high latitudes for the seasonal model as compared to the annual mean result. This result is consistent with the seasonal removal of the polar snowpack, which was mentioned previously.

In summary, the seasonal variation of solar radiation serves to remove the polar snowpack during the summer months. This reduces the earth's albedo in the polar regions at these times and allows more solar radiation to reach the ground there than in the case of annual mean insolation. This increased solar radiation, in turn, results in a warmer surface temperature at high latitudes in the seasonal model.

Oceanic Response

In section 4, we stated that the form of the oceanic depth temperature variations in middle to high latitudes (fig. 4) is influenced strongly by the combined effect of both forced vertical mixing and free convection. These mechanisms of oceanic heating and cooling have an interesting implication with regard to the mean ocean surface temperature in higher latitudes. As can be seen in the 60° latitude (upper) portion of figure 4, the onset of winter (December 1962 for the Northern Hemisphere) produces very little cooling of the surface layer (first 25–50 m) below the initial mean temperature (October 1962). During the onset of summer (June 1963 for the Northern Hemisphere), however, the temperature of the surface layer increases considerably above the initial value. This implies that, in this latitude region, the annual mean temperature of the ocean surface of the seasonal model is warmer than that for the annual mean model. In other words, the thermal response of the ocean to a seasonal variation of solar radiation produces a net warming of the higher latitude ocean surface to a value above the initial time-mean state. Figure 15, presented to clarify the reason for this warming, shows two configurations of oceanic temperature change. The right half of the diagram illustrates the heating and cooling of the surface layer to values above the mean deep-sea temperature, whereas the left half illustrates the cooling of the surface layer to a value below the deep sea value. In the first case, temperature changes of the surface layer are caused mainly by forced vertical mixing since this layer is stable with respect to free convection. Therefore, the surface temperature may be significantly increased during summer since most of the thermal energy involved goes into heating merely this relatively shallow surface layer. However, for the case of winter, both free convection and forced vertical mixing are present since buoyant instability results in convective mixing throughout the unstable layer. In this instance, the thermal energy involved must now be distributed over a deeper convective layer and, therefore, the temperature of the surface layer is not reduced to a value significantly below the annual mean or deep-sea value during the approach of winter. This type of oceanic response results in a warmer mean surface temperature and, therefore, warmer overlying air next to the ocean surface. This is an important factor in determining the resulting tropospheric temperature distribution over the ocean in high latitudes. This effect is most prominent in high oceanic latitudes where the convective layer is very thick during winter.

Since an equilibrium solution was not obtained, the discussion above applies only to the trend of the results shown. To ascertain that the oceanic warming described here is not a transient phenomenon, a very long-term integration of a one-dimensional diffusion model with the convective adjustment was performed. The results from this simple model imply that the oceanic heating process in high latitudes is an equilibrium effect rather than a transient one. The details of this computation are given in appendix 2.

For the 31° latitude case (middle portion of fig. 4), the approaching winter season produces a significant cooling

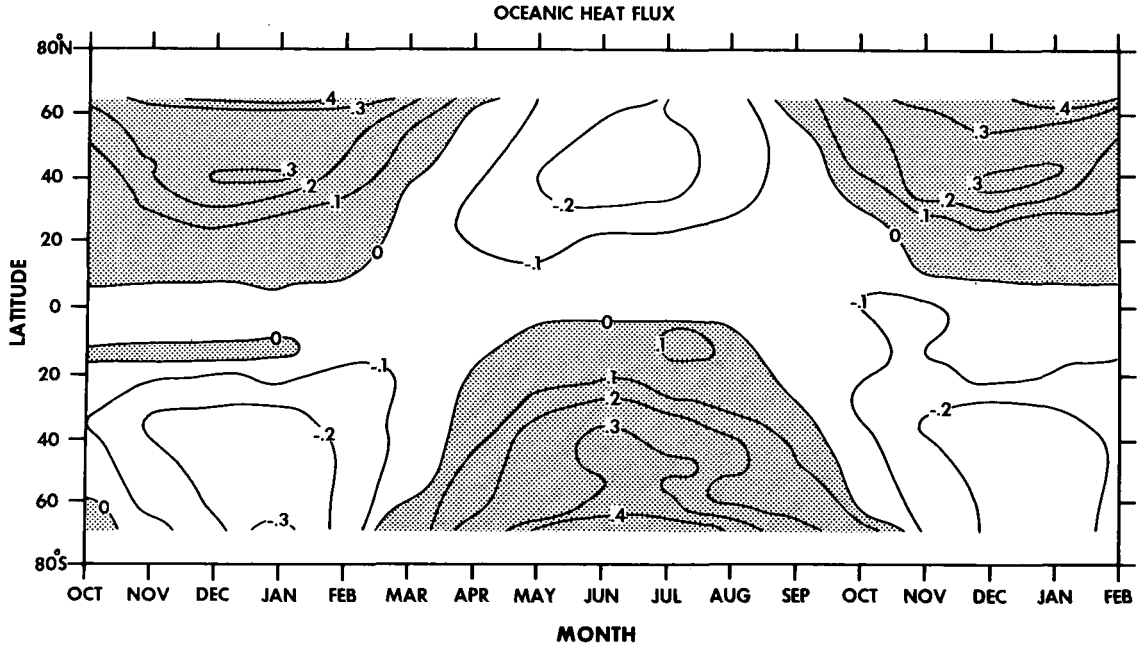

FIGURE 16.—Time variation of the heat flux from the interior to the surface of the ocean. Positive values indicate upward flux; negative values, downward flux. Units: ly/min.

of the surface layer below the initial mean temperature because the thickness of the convective layer at this latitude is less than that at 60° latitude. Therefore, the warming effect of the surface layer is considerably less than that obtained at 60° latitude.

In the 3° latitude case (lower portion of fig. 4), the situation is reversed. There is a reduction of the annual mean equatorial temperature throughout the surface layers. In other words, the ocean surface temperature of the seasonal model tends to be colder than that of the annual mean model in equatorial latitudes. According to our analysis, the surface equatorial zonal wind over the ocean is greater in the seasonal model than in the annual mean model. This would presumably create more upwelling in equatorial latitudes for the seasonal model. This cooling trend is reflected in the equatorial surface temperature difference shown in figure 10.

The convective activity of the ocean in high latitudes is reflected in the time variation of the zonally averaged heat flow from the interior to the surface of the ocean as shown in figure 16. Note that the absolute value of the oceanic heat flux in high latitudes is greater in winter than in summer. This is caused by the rapid convective mixing which predominates there during winter as compared to slower turbulent mixing which predominates during the summer.

We stated above that the major part of the warming is caused by removal of the polar snowpack during summer, with the seasonal variation of convective activity in the ocean in high latitudes contributing to a lesser degree. A rough estimate can be made concerning the relative contributions to this warming by referring to section 5 and figure 10. Figure 10 shows a surface temperature increase of 6°–10°K in the region from 55° to 65° latitude over the continent. The corresponding rise in surface temperature over the ocean in this latitude region is only 2°–3°K. Since the temperature of the atmosphere over the ocean is controlled mainly by the temperature of the ocean surface, this comparison gives a rough approximation to the relative effectiveness of the two mechanisms described above. Therefore, the snow cover effect appears to be the dominant process governing this warming whereas the effect of seasonal variation of oceanic convection appears to be only one-quarter to one-third as important. Above 66° latitude, the entire area of integration is treated as a continent and, therefore, one would expect the snow mechanism to dominate there regardless of other factors.

7. CONSEQUENCE OF WARMING

Many interesting features are evident in the seasonal model as a result of the warming trend in high latitudes, the most important of which is the reduction of mean meridional temperature gradient in both the atmosphere and ocean models as compared with the annual mean state. This section will briefly deal with three aspects of this difference.

Kinetic Energy of Transient Eddies

Figure 17 shows the horizontal distribution of vertically integrated mean eddy kinetic energy for the atmosphere for both the annual mean model and the seasonal model (left and right portions, respectively). The definition of this quantity is the same as that given in part I. This figure shows a considerable reduction of eddy kinetic energy for the seasonal model as compared with the annual mean model over most of the region except for the Tropics. The reason for this apparent decrease can be traced back to the mean decrease in tropospheric north–south temperature gradient resulting from the increased warming in higher latitudes, discussed in section 5. This implies a net

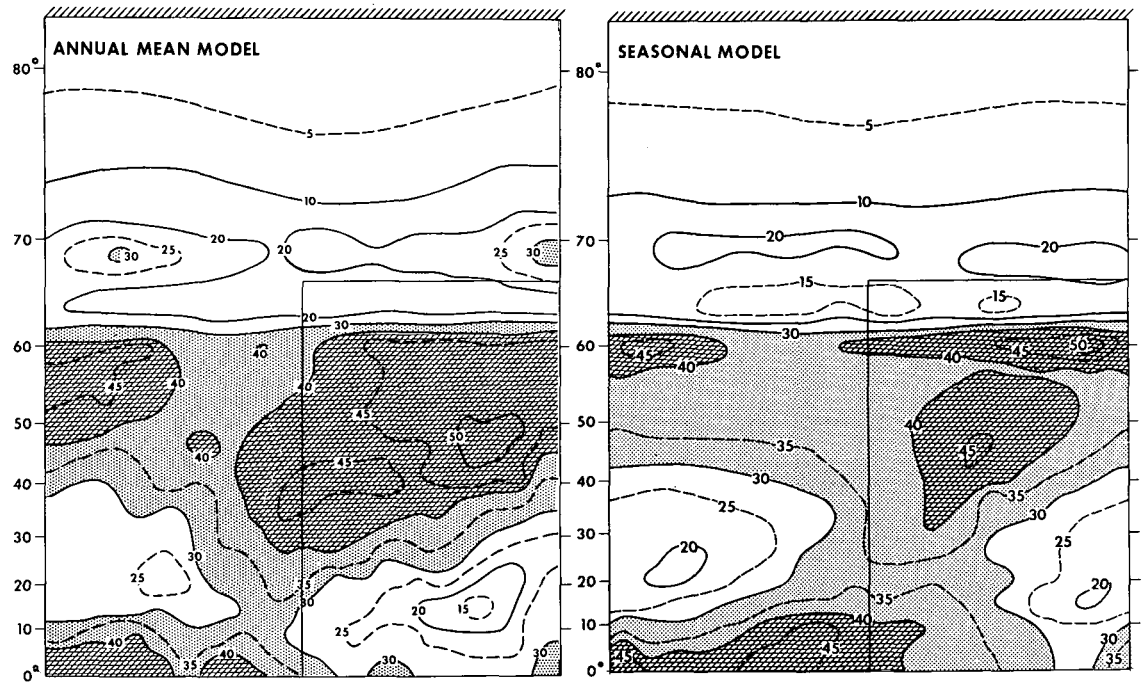

FIGURE 17.—Horizontal distributions of vertically integrated mean kinetic energy of transient eddies in the atmosphere for both the annual mean and the seasonal models. Averages are taken over the last full year for the seasonal integration. The values for the two hemispheres are also averaged. Units: $J \cdot cm^{-2}$.

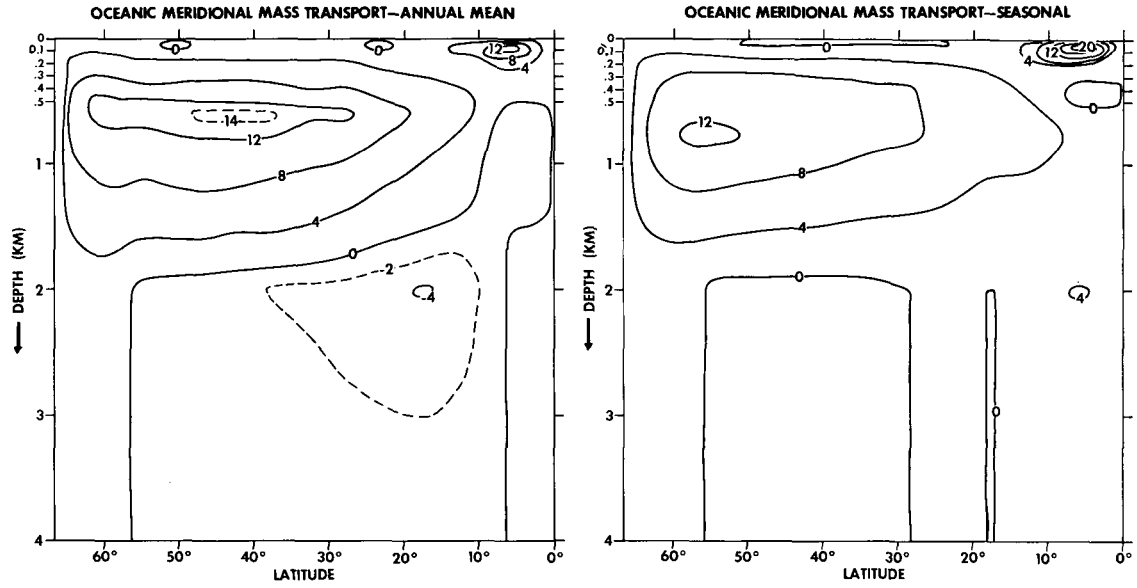

FIGURE 18.—Stream function of meridional circulation in the ocean. The averaging procedure is the same as that used for figure 17. Units: 1.0×10^{12} gm/s.

reduction in baroclinic instability and, hence, less storminess as a whole for middle and higher latitudes. This decreased north–south temperature gradient is also responsible for a net decrease in the poleward transport of total atmospheric heat energy by the seasonal joint ocean-atmosphere model in middle and high latitudes. This will be briefly discussed later in this section.

Note that the magnitude of eddy kinetic energy is unrealistically small in both the seasonal and annual mean atmospheres. As Manabe et al. (1970) show, the poor resolution of the horizontal finite differencing of the joint air-sea model is partly responsible for this discrepancy.

Oceanic Meridional Mass Transport

There is a counterpart to the reduced atmospheric meridional temperature gradient in the ocean circulation. Figure 18 shows the mean meridional oceanic circulation (mass transport) for both the seasonal and annual mean

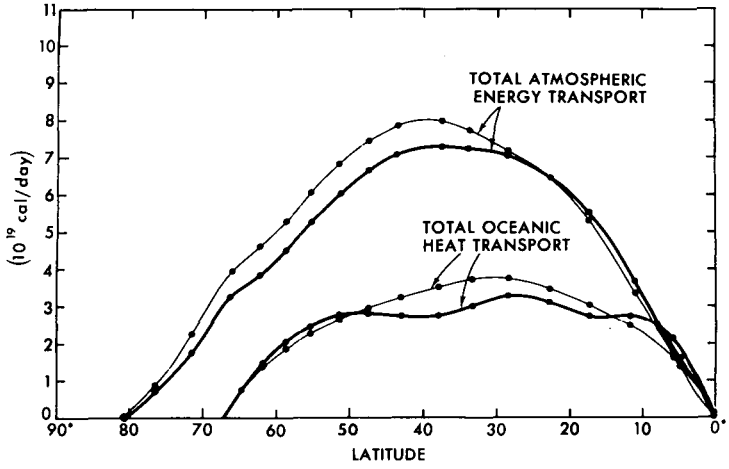

FIGURE 19.—Latitudinal distribution of the rates of poleward transport of atmospheric total energy ($c_pT+\Phi+k+L\cdot r$) and oceanic heat energy (H_o). Thick lines, seasonal model; thin lines, annual mean model. Units: 1.0×10^{19} cal/day.

models. According to this comparison, there is a general weakening of the meridional circulation of the seasonal model. Referring to the right-hand portion of figure 9, we see that a weaker meridional temperature gradient exists in the upper layers of the ocean as well as in the lower troposphere. This is due primarily to the warmer ocean surface temperature in high latitudes. Since the oceanic meridional circulation cell is thermally driven, this weaker temperature gradient results in a weaker oceanic meridional circulation.

Also shown in figure 18 is a slightly stronger tropical cell for the seasonal model. This implies a stronger upwelling at the Equator and, therefore, is consistent with the slightly colder surface temperature in equatorial waters. It should be noted that the meridional circulation in middle and high latitudes does not penetrate below 2-km depth because the deeper ocean is stable throughout the period of integration.

Poleward Transport of Energy

We mentioned earlier in this section that the decreased meridional temperature gradient from middle to high latitudes implies a decreased total poleward atmospheric heat energy transport in this region. Figure 19 shows the latitudinal distribution of this quantity for both the atmosphere and ocean separately. For the atmosphere, total energy is defined as the sum of heat energy ($c_pT+\Phi+k$) and latent energy ($L\cdot r$). The corresponding transport is computed by integrating the imbalance of various energy components from the Equator to the polar boundary. For the ocean, total meridional heat transport is computed by means of the formula

$$H_0=c_p\rho_0\{vT+A_H(\partial T/\partial\phi)a^{-1}\}$$

where c_p is specific heat of sea water, ρ_0 is density of sea water, v is meridional velocity, T is temperature, A_H is the coefficient of lateral diffusion, a is the radius of the earth, and $\{\}$ denotes an integral over longitude and depth.

Figure 19 shows a net decrease of the poleward atmospheric total energy transport of the seasonal model in middle to high latitudes as compared with the result from the annual mean model. This is consistent with the results already cited concerning eddy kinetic energy and meridional temperature gradient in this latitude belt. There is also a corresponding decrease of the oceanic heat energy transport of the seasonal model in middle latitudes. This is consistent with the weaker oceanic meridional circulation mentioned previously. The slightly larger oceanic heat energy transport obtained in the Tropics is due to the stronger tropical cell in the present seasonal integration.

8. SUMMARY AND CONCLUSIONS

In this study, an attempt is made to analyze the response of the joint ocean-atmosphere model to a seasonal variation of solar radiation and to compare these results with the annual mean state presented in part II. The latter was done to determine the effect of seasonal variation of insolation upon the climate and oceanic circulation. The most important fact resulting from this study is the significant increase in temperature which takes place in the lower troposphere at high latitudes. This temperature increase was analyzed and found to be mainly caused by two factors:

1. The removal of the snowpack during the summer months, which in turn reduces the albedo of the earth's surface at high latitudes during this season. This allows more solar radiation to be absorbed by the ground there than is possible in the annual mean case, where snow cover persists throughout the entire period of integration; and
2. The net warming of the surface layer of the ocean in high latitudes which increases the overlying air temperature there. This net warming is caused by the seasonal variation of convection in the surface layer of the ocean.

It is difficult to assess the exact relative contributions to the high-latitude tropospheric temperature increase by these two effects separately. However, the present results indicate that the removal of snow cover during the summer seasons is the primary cause of this warming, whereas the oceanic effect appears to be secondary in importance or about one-fourth to one-third as much in magnitude.

It is interesting to compare the results of the present seasonal study with the theory of climatic change advanced by Milankovitch (1941) concerning the secular variations of solar radiation and snow cover caused by changes in the orbital parameters of the earth. According to his calculations, periods of cool summers are considered to favor ice-age cycles whereas periods of warm summers are considered to favor interglacial or warm cycles. Since the trend of the present seasonal computation indicates a warmer tropospheric temperature in high latitudes as compared with the case of annual mean insolation, the results are relevant to this particular aspect of the Milankovitch theory. However, the present results indicate that both snow accumula-

tion during the winter season and heating during the summer season may be important in determining whether or not the polar snowpack will survive a given yearly cycle. In the Milankovitch model, the snow cover (snow altitude) is considered to be a function of only the summer insolation and not of the winter or annual mean insolation.

The results of the present study suggest that the incorporation of a seasonal variation of solar radiation produces a warmer climate in higher latitudes of the model. However, a quantitative estimate of this effect must await the inclusion of various other factors in the model. One of these factors is replacement of the present climatological distribution of water vapor by the predicted distribution of this quantity for the computation of radiative transfer. According to a study by Manabe and Wetherald (1967), "this radiation–water vapor coupling" may be expected to almost double the sensitivity of the temperature of the model atmosphere to changes in the solar constant. The incorporation of this coupling could quantitatively modify the warming effect presented for this current seasonal study. Another factor of importance may be the relative size of the continent versus that of the ocean. An increase of the continental area would increase the amplitude of the seasonal variation of surface temperature and accordingly may be expected to further amplify this atmospheric warming. Also, it should be recalled here that the cloudiness adopted for this study was held fixed and did not vary with time. The effect of seasonal variation of cloudiness could alter the quantitative aspects of the present results.

It would be desirable to increase the resolution of the present air-sea model. The results of a study by Manabe et al. (1970) indicate that an increase of horizontal resolution provides an improved description of the atmospheric features. In particular, the air-sea tropical rainbelt and tropical circulation would be better represented than they are at present.

Finally, it should be reemphasized that, because a true equilibrium was not reached, the present result does not represent a final mean temperature state for the seasonal model. However, the trend of the results and the test computation shown in appendix 2 indicate that the incorporation of a seasonal variation of insolation would result in a warmer atmosphere than is obtained with an annual mean insolation.

APPENDIX 1: SEASONAL VARIATION OF RADIATION INPUT

Solar Radiation

In this model experiment, the mean cosine of the zenith angle of the sun and the daylight fraction are made functions of latitude and the declination of the sun. The declination of the sun changes roughly sinusoidally throughout the year and may be obtained from astronomical tables. To avoid interpolation inaccuracies and the large computer storage required by the use of tables, we incorporated into the model a simple program for solving the basic celestial mechanics equations of the earth's orbit. The solutions to these equations yield the solar declination and distance to the sun in astronomical units (radius vector), given the date. This procedure is approximate, but it gives the declination to within 1 min of arc and the radius vectors within one part in 20,000.

The mean cosine of the zenith angle is computed by integrating the equation for the instantaneous zenith angle, Z given below, over all hour angles:

$$\cos Z=\sin \phi \sin \delta+\cos \phi \cos \delta \cos h \qquad (1)$$

where ϕ is latitude, δ is declination, and h is hour angle. Setting $Z=90°$ in eq (1), we obtain the hour angle, H, of the sun at sunrise or sunset, which is

$$H=\cos^{-1}(-\tan \phi \tan \delta).$$

The fraction, F, of sunlight during the day is

$$F=H/\pi.$$

The integration of eq (1) from $h=-\mathrm{H}$ to $\mathrm{h}=+\mathrm{H}$, or over hours of daylight, gives the time mean of the cosine of the zenith angle; namely,

$$\overline{\cos Z}=\sin \phi \sin \delta+(\cos \phi \cos \delta \sin H)/H.$$

This integration is performed under the assumption of constant δ during roughly half of a day, a very good approximation during most of the year. (The maximum rate of change of δ is less than half a degree per day, occurring in the spring and fall.) The mean cos Z is corrected for the variable distance from the earth to the sun by dividing it by the square of the radius vector.

Atmospheric Absorbers

The mixing ratio for water vapor and the ozone concentration are also made to vary with season. The mixing ratio for water vapor varies sinusoidally from a Northern Hemisphere maximum in July to a minimum in January; and the ozone concentration from a Northern Hemisphere maximum in April to a minimum in October. The nodes for the sinusoids are chosen to occur approximately at the equinoxes for the water vapor interpolation and approximately at the solstices for the ozone interpolation. The extremes are the climatic means for these four months. (See part I for the source of these data.) In the Southern Hemisphere, the phases of these variations are reversed.

APPENDIX 2: A SIMPLE TEST OF OCEAN SURFACE WARMING

In section 6, we stated that the seasonal variation of convective activities in the surface layer of the ocean in high latitudes was responsible for the warming that occurred there. To determine whether this oceanic warming represents an equilibrium state or a transient one, we simulated this process in a simple vertical diffusion model integrated over a long time period. The usual one-

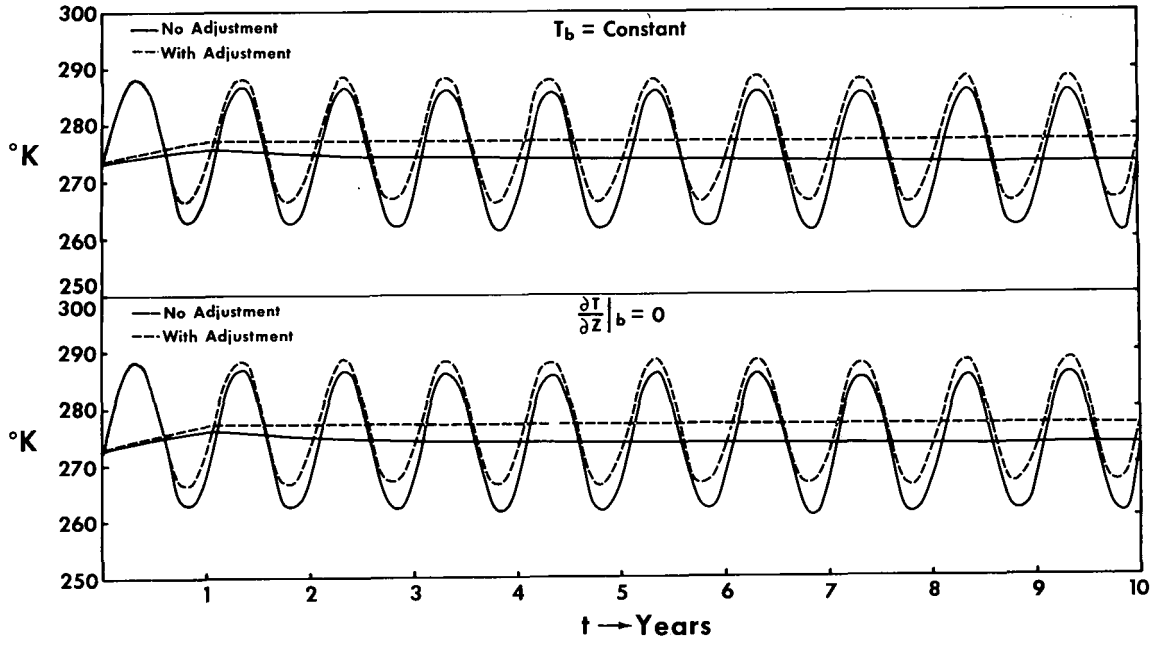

FIGURE 20.—Time variation of surface temperature (°K) for the first 10 yr of integration of the one-dimensional diffusion model for (top) fixed bottom temperature and (bottom) zero bottom heat flux. Solid lines indicate runs made with a convective adjustment; dashed lines indicate runs made without a convective adjustment. The subscript "b" denotes bottom.

dimensional heat diffusion equation was used for this test computation, namely,

$$\frac{\partial T}{\partial t}=K\frac{\partial^2 T}{\partial z^2}$$

where T is temperature, K is thermal diffusivity, t is time, and z is depth. In this model, K is considered to be constant except for the case of free convection, when it is assumed to become infinite. To simulate free convection, a "convective adjustment" is introduced into the model. The convective adjustment is such that if an unstable stratification is predicted, the computed values of temperature are adjusted so that the vertical temperature gradient vanishes. Total energy is assumed to be unaltered by this adjustment. The computations of vertical mixing and the convective adjustment are identical with those performed for the oceanic portion of the seasonal model except that variations of salinity are not taken into consideration.

A sinusoidal heat flux with zero running-mean over an annual cycle is imposed at the surface. Two choices of bottom boundary conditions are used, (1) fixed temperature and (2) zero heat flux. The latter condition corresponds to the one used for the ocean computation.

The amplitude of the surface heat flux was set equal to 0.3 ly/min. This value falls well within the variation of the ocean surface heat flux in high latitudes presented in figure 16. The vertical thermal diffusivity was given the same value as that used for the ocean calculation, 1.5 cm^2/s. Total depth was 4 km with the same vertical finite difference structure as that used for the oceanic computation of the seasonal model. Initial conditions in all cases consisted of an isothermal temperature profile (273°K).

The result of integrating the diffusion model with a convective adjustment is to be compared with that obtained without the use of a convective adjustment. This latter computation will provide a standard for evaluating the effect of the convective adjustment upon the final equilibrium temperature profiles for both cases of bottom boundary conditions.

Figure 20 shows the time history of surface temperature with and without an adjustment for the first 10 yr of integration. The upper portion corresponds to the case with a fixed bottom temperature whereas the lower portion corresponds to the case of zero heat flux at the bottom. The lines, drawn through the centers of the sinusoidal curves, indicate the average running-mean surface temperature over each yearly cycle which correspond to the separate runs. According to this figure, the mean surface temperature for the separate runs made with a convective adjustment is generally higher than for the runs made without this adjustment. This increase in mean temperature is also indicated by the displacement of the sinusoidal curves themselves. In general, there appears to be little difference between the two cases with different bottom boundary conditions.

The final annual mean equilibrium temperature profiles obtained at the end of the four trials are shown in figure 21 for the first 500 m of depth. The values below this point are identical with those shown at the 500-m level. The runs with a convective adjustment arrived at an equilibrium state after approximately 200 yr whereas the run without a convective adjustment took roughly 3,000–8,000 yr to reach this state. The longest time corresponds to the fixed bottom temperature case without an adjustment. The total period of integration in all cases was 10,000 yr.

Figure 21 clearly shows the surface layer warming for the cases with an adjustment as compared to the cases

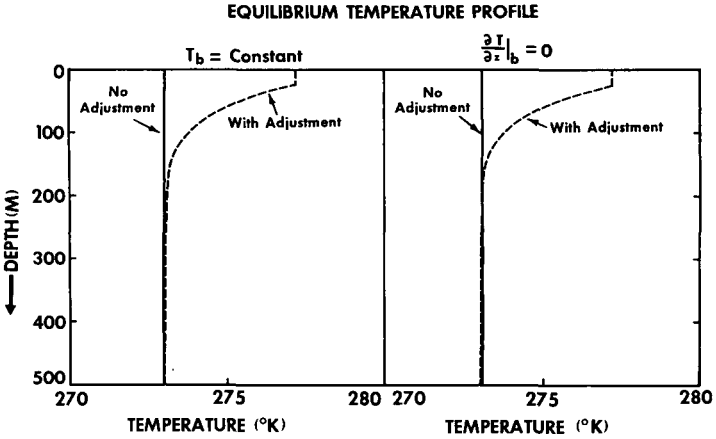

FIGURE 21.—Final temperature profiles (°K) for the upper 500-m ocean depth obtained from the one-dimensional diffusion model: (Left) fixed bottom temperature and (right) zero bottom heat flux. Values below 500-m depth are omitted for the purposes of scaling along the ordinate. The small vertical portion at the top of the curves corresponds to the surface wind layer. The same graphical conventions are used as in figure 20.

without an adjustment. This temperature difference at the surface is about 4°K. It is also evident that this warming is confined strictly to the upper 150 m of the fluid. This result is comparable with the discussion presented in section 6 concerning the oceanic warming in high latitudes. Throughout the calculation, checks were made to insure energetic consistency of the various systems. Fourteen digit accuracy was used to reduce roundoff errors that otherwise occur during such an extended time integration. Also, no significant changes in the results occurred when the vertical resolution of the model was increased.

In summary, the results of this test tend to support the hypothesis that the oceanic warming discussed in section 6 is an equilibrium phenomenon rather than a transient one. However, care must be taken in interpreting these results literally because of the other nonlinear interactions present in the air-sea model which tend to modify this process. In particular, the surface oceanic heat flux can change as a result of the increase in ocean surface temperature. This feature is not included in this idealized model.

ACKNOWLEDGMENTS

As is the case in any project of this nature, several people aided or contributed to the completion of this study. The authors gratefully acknowledge the assistance given by Kirk Bryan who constructed the ocean model and who contributed greatly to the subsequent evaluation of the results. The authors are grateful to J. Leith Holloway, Jr., for preparing the astronomical computation and incorporating it into the joint model.

We also wish to thank David Durdall for programming the increase in the number of vertical levels in the ocean model, Michael D. Cox for assisting with the ocean portion of the seasonal analysis, and Douglas J. Johnson for supervising the running of the seasonal model.

Finally, thanks are due William H. Moore and Philip G. Tunison for preparing and drafting the figures and Monika Stern for typing the manuscript.

REFERENCES

Bryan, Kirk, "Climate and the Ocean Circulation: III. The Ocean Model," *Monthly Weather Review*, Vol. 97, No. 11, Nov. **1969**, pp. 806–827.

Budyko, M. I. (Editor), *Atlas Teplovo Balansa Zemnogo Shara* (Guide to the Atlas of the Heat Balance of the Earth), Gidrometeoizdat, Moscow, U.S.S.R., **1963**, 69 pp.

Kidson, John W., Vincent, Dayton G., and Newell, Reginald E., "Observational Studies of the General Circulation of the Tropics: Long Term Mean Values," *Quarterly Journal of the Royal Meteorological Society*, Vol. 95, No. 404, London, England, Apr. **1969**, pp. 258–287.

Manabe, Syukuro, "Climate and the Ocean Circulation: I. The Atmospheric Circulation and the Hydrology of the Earth's Surface," *Monthly Weather Review*, Vol. 97, No. 11, Nov. **1969***a*, pp. 739–774.

Manabe, Syukuro, "Climate and the Ocean Circulation: II. The Atmospheric Circulation and the Effect of Heat Transfer by Ocean Currents," *Monthly Weather Review*, Vol. 97, No. 11, Nov. **1969***b*, pp. 775–805.

Manabe, Syukuro, and Bryan, Kirk, "Climate Calculations With a Combined Ocean-Atmosphere Model," *Journal of the Atmospheric Sciences*, Vol. 26, No. 4, July **1969**, pp. 786–789.

Manabe, Syukuro, Smagorinsky, Joseph, Holloway, J. Leith, Jr., and Stone, Hugh M., "Simulated Climatology of a General Circulation Model With a Hydrologic Cycle: III. Effects of Increased Horizontal Computational Resolution," *Monthly Weather Review*, Vol. 98, No. 3, Mar. **1970**, pp. 175–212.

Manabe, Syukuro, and Strickler, Robert F., "Thermal Equilibrium of the Atmosphere With a Convective Adjustment," *Journal of the Atmospheric Sciences*, Vol. 21, No. 4, July **1964**, pp. 361–385.

Manabe, Syukuro, and Wetherald, Richard T., "Thermal Equilibrium of the Atmosphere With a Given Distribution of Relative Humidity," *Journal of the Atmospheric Sciences*, Vol. 24, No. 3, May **1967**, pp. 241–259.

Milankovitch, Milutin, "Kanon der Erdbestrahlung und seine Anwendung auf das Eiszeitenproblem" (Canon of Radiation on Earth and Its Application to the Ice-Age Problem), *Académie Royale Serbe Edition Spéciales*, No. 132, Belgrade, Yugoslavia, **1941**, 633 pp.

Oort, Abraham H., and Rasmusson, Eugene M., "On the Annual Variation of the Monthly Mean Meridional Circulation," *Monthly Weather Review*, Vol. 98, No. 6, June **1970**, pp. 423–442.

Robinson, Margaret K., "Sea Temperature in the North Pacific Area, 20°–40°N, 125°–155°W," *Task Report* VI, Contract No. N6ori–III, Scripps Institution of Oceanography, La Jolla, Calif., Sept. 15, **1951**, 14 pp.

Robinson, Margaret K., "Sea Temperatures in the Gulf of Alaska and in the Northeast Pacific Ocean, 1941–1952," *Bulletin of the Scripps Institution of Oceanography*, Vol. 7, No. 1, La Jolla, Calif., **1957**, pp. 1–98.

Sverdrup, Harald Ulrik, Johnson, Martin W., and Fleming, Richard H., *The Oceans, Their Physics, Chemistry and General Biology*, Prentice-Hall, Inc., New York, N.Y., **1942**, 1087 pp.

[*Received March 25, 1971; revised June 28, 1971*]